PRESSURE RATIO IMPACT ON COMPRESSIBLE FLUID FLOW THROUGH A LASER DRILLED SINGLE ORIFICE RESTRICTOR

(THEORETICAL AND ACTUAL EDGE CONDITIONS)

Ian Navin

Engineering Project
Submitted in Partial Fulfillment of the Requirements for the Degree of

Master of Engineering in Mechanical Engineering

Approved by:
Dr. Francisco Cunha, PhD, PE

Department of Mechanical, Aerospace, and Nuclear Engineering
Rensselaer Polytechnic Institute
Troy, New York

[December 2022]

Submitted July 2022

TABLE OF CONTENTS

LIST OF SYMBOLS

a	Acoustic Speed or Speed of Sound
a_o	Speed of Sound - Stagnation
a^*	Speed of Sound - Critical
a	Acceleration
A	Area
B	Body Force
C_d	Coefficient of Discharge
c_p	Specific Heat at Constant Pressure
c_v	Specific Heat at Constant Volume
D	Drag Force
e	Specific Stored Energy
E	Stored Energy
F	Force
F_c	Compressibility Factor
g	Gravity
G	Mass Flux
γ	Specific Heat Ratio
h	Specific Enthalpy
i, j, k	Unit vectors in x, y, and z directions
I	Volumetric Flow (SCFM)
m	Mass
$\dot{m}$	Mass Flow Rate
M	Mach Number
M	Momentum
p	Pressure
P	Stagnation pressure
p^*	Critical Pressure
ρ	Density
ρ_o	Stagnation Density
ρ^*	Critical Density
Q	Heat
R	Gas Constant
s	Specific Entropy
S	Entropy
t	Temperature
T	Stagnation Temperature
t^*	Critical Temperature
u	Specific Internal Energy or Velocity in x
U	Internal Energy
$\mathcal{V}$	Specific Volume
v	Velocity in y
V	Volume
V	Velocity

w	Velocity in z
W	Work
Ω	Flow Resistance

LIST OF TABLES

LIST OF FIGURES

ABSTRACT

The study of a one-dimensional isentropic compressible flow through a single orifice has been conducted starting with the theory and background of fluid and gas dynamics. Of interest is the impact of the pressure ratio on a precision orifice restrictor measuring at 0.0007” as the desire for efficient and highly restrictive orifices that operate in the sonic vs the subsonic region in propellant management systems is in high demand. When exploring the theoretical impact, a coefficient of discharge of a sharp edge orifice (0.61) was used. When producing a precision orifice using a laser system, the edge condition was unknown, but through experimental flow testing was found to be around 0.65 in the sonic region and 0.61 in the subsonic region when using a 100 psia inlet pressure. The critical pressure ratio is theorized at approximately 1.9 and with experimentation was found to be valid with some minor error. This error is concluded to be from the assumptions and one-dimensional analysis conducted or the inaccuracies of the equipment used to perform the flow testing. It appears that the transition between the sonic and subsonic region is not as abrupt as the theory portrays, rather, there is more of a transition region that could be explored in more depth.

1. INTRODUCTION

1.1 Project Background

Precision fluid flow has recently expanded to pneumatic systems for the space industry. These space applications require the precision fluid metering for systems such as ion propulsion. With the limited capacity to store fuel such as Krypton and Xenon, the efficiency is critical. These systems utilize precision fluid flow elements like sharp edge orifice restrictors to meter flow. One way to ensure efficiency of a system is to have known characteristics of the fluid flow such as sonic or subsonic conditions at the orifice. Subsonic flow occurs when the Mach number is less than one and is difficult to predict the performance. Sonic flow conditions are achieved when the Mach number is equal to one where the flow is said to be choke. The pressure ratio of the downstream pressure to upstream pressure for a sonic condition is approximately $\frac{P_2}{P_1} = 0.53$ or $\frac{P_1}{P_2} = 1.9$ and results in a constant flow rate independent of the downstream pressure. Since a constant flow rate is predictable, space applications aim to maintain the sonic condition. Exploring the impact of the pressure ratio on a single orifice restricting element will help characterize the performance and aid in the design of the element in both the sonic and subsonic regions.

Propulsion systems such as an Ion thruster use inert gasses and electrical power to propel the crafts in space. When the electrons collide with the neutral propellant atom, ionization occurs and a positively charged ion is created. The ions are then propelled through the charged grids at the end of the chamber. The neutralizer, or the cathode, emit more electrons to neutralize the positively charged ions that pass through the charged grid. The thrust produced is very low, but overtime, can reach high velocities, “90,000 meters per second (over 200,000 mph)” [13] which is ideal for

environments such as space. Efficiency of the thruster can be linked to the precision fluid flow of the anode and cathode (or neutralizer) in the propellant management system. The control of the anode and cathode must be precise as to ensure fuel isn't being wasted. On the other hand, with the wrong ratios, the efficiency will suffer. The best way to predict that precision flow, is through a highly restrictive component that will operate in the sonic region for as long as possible. This will yield a more consistent and predictable flow inside and outside the discharge chamber. Many times, the high restriction is achieved with multiple orifices, but a small orifice can also be used if small enough though cleanliness can become an issue. Manufacturing an orifice to the required restriction can be a challenge, but with a laser, the feat is attainable. Understanding the theory behind the compressible fluid flow in both the sonic and subsonic state through a highly restrictive orifice plate will be the foundation for manufacturing and designing orifice plates in the future while also comparing to experimental data to compare the accuracy and identify the losses.

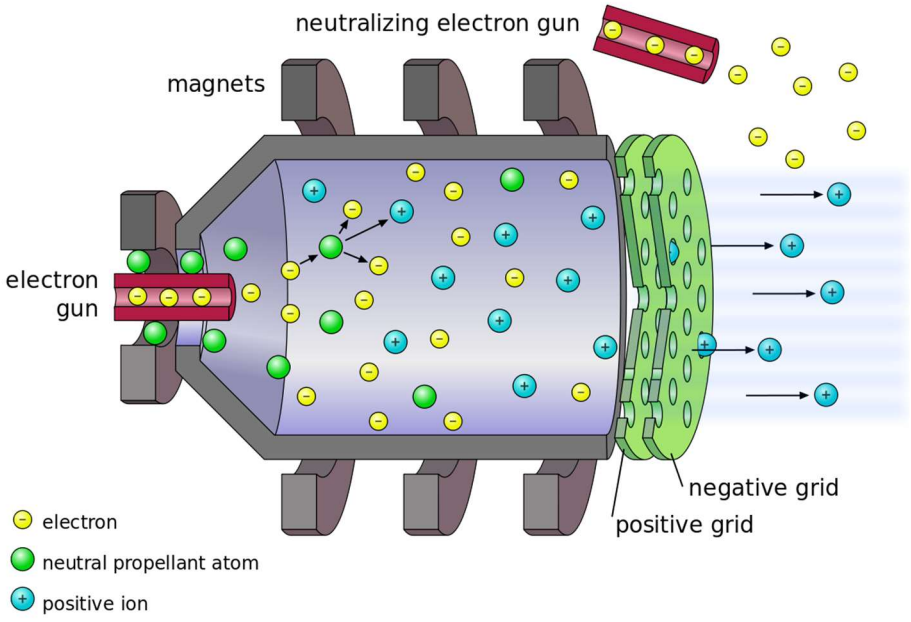

Figure 1: Ion Thruster (Anode and Cathode) [13]

1.2 Assumptions

To accurately solve this problem theoretically, we must consider some assumptions. We will be looking at a steady one-dimensional inviscid compressible fluid flow with a constant sharp metal orifice geometry including the diameter (0.0007" with a max thickness of 0.0055"). We will also consider an isentropic flow which assumes an adiabatic and reversible flow and expansion through the orifice. In this type of flow, the work transfer of the system is frictionless, and no net transfer of heat or matter will occur. The fluid and surrounding bodies are in thermal equilibrium. We also assume that no condensation at the orifice occurs or any effects of radiation.

When an inlet pressure is applied, we will consider this pressure to be constant. This also applies to any downstream pressure considered. We assume that the lowest downstream pressure is atmosphere (14.7 psia). The largest upstream pressure to be considered will be 100 psia (yielding a max pressure ratio ($\frac{P_1}{P_2}$) of 6.8). The calculations will consider nitrogen gas and future work can include many other gases for correlation.

For the experimental testing, a flowmeter must be used which can induce its' own backpressure on the system. The flowmeter will be kept downstream of the orifice as to not over pressurize the flowmeter. The placement of the flowmeter will induce backpressure to the system which will be monitored by the downstream pressure gauge. The backpressure will be monitored and compared to atmospheric pressure. We also will assume that the flow system is free of leaks and that the nitrogen gas used is at least 99.9% pure. In the pressure gauges, flowmeter, and thermocouple, there is inherent measurement accuracy which will be considered (0.5% Reading).

1.3 Previous Work

Previous work has been achieved by many using some of the same methodologies, but not with all methods combined as the scale that these calculations and experiments were performed are much smaller than previous work researched. Theory is well described and followed closely from Zucrow's Gas Dynamics text [1] which theorizes the behavior of compressible fluids.

The study in the following body uses a laser drilled single orifice with a size of 0.0007" on Nitrogen gas. The smallest hole size of a sharp edge orifice drilled in a metal plate is 0.004" and 0.0012" in a sapphire restrictor performed by O'Keefe Controls Co [6] both tested on air. It was found that the flow at 90 psig (104.7 psia) was 0.6 and 0.053 SLPM respectively. The restriction provided by the 0.0007" orifice along with the edge conditions and manufacturing methods make this study unique. Definition of the mass flow in terms that utilize the coefficient of discharge along with the area is derived and follows similarly to the restriction of an orifice defined in Lohms [3,4]. It is of interest with this high restriction and corresponding orifice size if the gas dynamics theory can be utilized accurately to predict the mass flow and behavior of the fluid based upon the edge conditions and the pressure ratio.

Other work was performed for a metal drilled orifice to study the discharge coefficient back in 1988 by C.H. Kurita [14]. This study utilized theory from Mark's Handbook for Mechanical Engineers [2] and larger drilled orifices down to 0.05" on Nitrogen gas. The study also used equipment dated for the period with a rotameter for the flow measuring device, which does not yield the accuracy of modern flowmeters.

2. CONCLUSIONS

The purpose of this report is to analyze the flow of a compressible fluid through a miniature sharp edge orifice in theoretical and experimental fashion. This study would allow the understanding of the behavior of the restricted fluid flow under many pressure conditions which allows a more precise design of the orifice for use in propellant management systems.

After detailing the governing equations, the assumptions were applied to arrive at the simplest form of the equations to use for the theoretical analysis. After applying the known discharge coefficients and target orifice size (0.0007”) to the sonic and subsonic flow rate equations, curves were drawn to show, theoretically, how the compressible fluid should behave in the orifice depending on the inlet and outlet conditions, most notably the pressure ratio of the upstream and downstream pressures as seen in Figure 8. An equivalent size orifice (0.0007”) was produced using a laser to mimic the smallest orifice that the laser could make. The vision system was used to measure the orifice and observe the form to aid in analysis of the edge conditions. After flow testing the orifice plate at differing pressure ratios with a constant upstream pressure of 100 PSIA, a pressure ratio vs flow rate curve was drawn and compared to the theoretical flow of a sharp edge and a round edge hole as shown in Figure 16. The 0.0007” laser drilled hole agreed more with the sharp edge orifice in the subsonic region with a percent difference of approximately 1.9%. With an adjustment of 0.04 of the coefficient of discharge, the sonic region agreed better with a percent difference of 0.72%, though this compromised the agreement in the subsonic region to a percent difference of 5.75%. The comparison of the experimental and the adjusted coefficient of discharge can be seen in Figure 17. It was observed that at the apparent sonic/subsonic boundary, the flow rate did not stay constant as the theory concludes. The flow rate in the sonic region agreed mostly,

but slowly decreased until the pressure ratio of approximately 1.9. This may be due to the many assumptions made of the fluid such as the fluid was adiabatic, frictionless, reversible, and perfect.

When moving forward to design the miniature precision orifices using this type of laser, the coefficient of discharge of a theoretical sharp edge orifice can be best used for theoretical calculations. It should also be noted that the sonic and subsonic boundary layer is not as abrupt as the theoretical calculations and theory would show, rather, there is a transition region before and after the pressure ratio of 1.9. In the sonic region, the flow does appear to experimentally remain constant, but does still increase slightly as the pressure ratio increases. This can be taken into consideration if designing precision systems that will operate in the sonic region.

3. ANALYSIS

To be able to solve a gas dynamics problem, we must first understand the fundamentals of fluid dynamics. The following equations and derivations were closely followed by the Gas Dynamics text by Maurice Zucrow [1], though these derivations have been completed in many other texts and sources.

3.1 Fundamentals and Background

These fundamentals can be summarized in the form of essential equations of the Conservation of Mass, Momentum, and Energy. We also must initially consider the second law of thermodynamics to define the entropy and the thermodynamic properties of the fluid in question. From these basic governing equations, we can further simply by applying our assumptions and boundary conditions. This will yield manageable equations that will, to an extent, describe the fluid flow through the orifice depending on the inlet and outlet conditions of the fluid. The integral forms can first be derived as they can be applied to any type of fluid flow situation. Differential forms of these equations may be derived as well by utilizing the divergence theorem, but we will be utilizing the integral forms for this study.

Starting with the conservation of mass, it is stated that for a constant density fluid within a control volume, the mass is conserved. In other words, whatever enters the control volume, must also leave that control volume, $\mathcal{V}$. It is shown that the integral form of the Conservation of Mass takes the form of

$$\int_{\mathcal{V}} \frac{d\rho}{dt} d\,\mathcal{V} + \int_{A} \rho d\mathcal{V} \cdot dA = 0 \tag{1}$$

When considering a steady flow, the first term of the equation will equal zero.

$$\int_{A} \rho d\mathcal{V} \cdot dA = 0 \tag{2}$$

Moving to the Momentum Equation, we start with Newton's Second Law of Motion which states

$$F_{external} = \frac{dM}{dt} = \frac{DM}{Dt} \tag{3}$$

If we let $= \boldsymbol{M} = \int_{\mathcal{V}} \boldsymbol{V} \rho d\mathcal{V}$ *and* $n = V$, and use the subscript, t, as the partial derivative with respect to time, then

$$F_{external} = \int_{\mathcal{V}} (\rho \boldsymbol{V})_t dV + \int_{A} \boldsymbol{V}(\rho \boldsymbol{V} \cdot d\boldsymbol{A}) \tag{4}$$

When considering the control volume, we look at the net forces acting on the volume which is the addition of the body, F_B and surface forces, F_S where the body forces include gravity or other magnetic forces, and the surface forces include the normal and tangential forces on the body. With this we can say

$$F_{external} = F_B + F_S \tag{5}$$

$$F_B = \int_{\mathcal{V}} \boldsymbol{B} \rho \, dV \tag{6}$$

$$F_S = F_n + F_t \tag{7}$$

For an inviscid fluid flow, the shear forces acting on the control volume do not exist, so the surface forces considered when dealing with inviscid fluid flow is negligent. When looking at the tangential force, the surface has a compressive stress which yields a negative force sign where

$$F_n = -\int_A p\, d\boldsymbol{A} \tag{8}$$

Which makes the external force equation

$$\boldsymbol{F}_{external} = \int_{\mathcal{V}} \boldsymbol{B}\rho\, dV - \int_A p\, d\boldsymbol{A} \tag{9}$$

And the Integral form of the Momentum Equation acting in three components of x, y, and z

$$\int_{\mathcal{V}} \boldsymbol{B}\rho\, dV - \int_A p\, d\boldsymbol{A} + \boldsymbol{F}_{shear} = \int_{\mathcal{V}} (\rho \boldsymbol{V})_t dV + \int_A \boldsymbol{V}(\rho \boldsymbol{V} \cdot d\boldsymbol{A}) \tag{10}$$

Since we are considering the flow in the x direction, we can apply the x components, $n_i, B_i, and\ u_i$

$$\int_{\mathcal{V}} \boldsymbol{B_i}\rho\, dV - \int_A p n_i\, d\boldsymbol{A} + n_i \cdot \boldsymbol{F}_{shear} = \int_{\mathcal{V}} (\rho u_i)_t dV + \int_A u_i(\rho \boldsymbol{V} \cdot d\boldsymbol{A}) \tag{11}$$

And for steady flow conditions, $\int_{\mathcal{V}} (\rho u_i)_t dV = 0$.

Looking next at the energy equation, we start with the first law of thermodynamics which states that the change in stored energy of a fluid is equal to

$$de = \delta Q - \delta W \tag{12}$$

Where $Q = heat$, $W = work$, and $e = u + \left(\frac{V^2}{2}\right) + gz$. The integral form of the energy equation is found by evaluating what makes up the heat in a control volume (conduction, convection, and radiation) and the total work done by the fluid which includes the work done by the normal forces over the surface.

$$\dot{W}_{shaft} + \dot{W}_{shear} - \dot{Q} + \int_{\mathcal{V}} \frac{\partial}{\partial t} [\rho \left(u + \left(\frac{V^2}{2}\right) + gz\right) d\mathcal{V} + \int_A [\rho \left(h + \left(\frac{V^2}{2}\right) + gz\right) (\rho \boldsymbol{V} \cdot d\boldsymbol{A}) = 0 \tag{13}$$

Lastly, the second law of thermodynamics which considers entropy, s, of the system. Because we are dealing with a Reversible process, it is shown that for a system

$$ds = \frac{\delta Q}{t} \tag{14}$$

If we consider the mass of a system, we can say that the total entropy, S is ms. After applying the time rate of change in entropy of the system $\frac{DS}{Dt} = \frac{\delta \dot{Q}}{t}$, we obtain the integral form of the entropy equation.

$$\int_{\mathcal{V}} (s\rho)_t d\mathcal{V} + \int_A s(\rho \boldsymbol{V} \cdot d\boldsymbol{A}) = \frac{\dot{Q}}{t} \tag{15}$$

Where $(s\rho)_t = \frac{\partial (sp)}{\partial t}$ and $\dot{Q} = \int_V \delta \dot{Q}$. Note that the subscript, t, denotes the derivative with respect to time, $\frac{d\rho}{dt}$.

3.2 One-Dimensional Steady Flow

With the integral forms of the governing equations described, we can see that they can be tough to manage, so we will apply our assumptions to the equations which will make them less complex. Using the following assumptions has been stated to yield very accurate results for internal flows [1].

The first assumption to apply is that the flow is steady, meaning that the flow properties and conditions do not change with time, though practically speaking most flows are not steady since they experience turbulence and eddies. The second assumption is that we are dealing with a one-dimensional flow, so that the properties of the fluid are uniform at every location that the fluid

mass crosses the control surface. Lastly, we will neglect the effects of body forces, which can be justified for a compressible flow where the body forces are typically insignificant.

First, we will consider the steady flow through a tube as shown in Figure 2 [1].

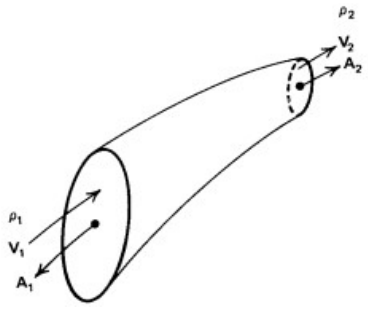

Figure 2: Generic Stream Tube [1]

Applying the Conservation of mass through this stream tube, we first take the integral form of the equation as stated in equation 1 and apply the steady flow condition which yields equation 2. Applying equation 2 to the properties shown in Figure 2, yields

$$\int_{A_1} \rho d\mathcal{V} \cdot dA + \int_{A_2} \rho d\mathcal{V} \cdot dA = 0 \tag{16}$$

By integrating we obtain the mass flow rate through the stream tube, which can be applied to any type of one-dimensional flowing fluid.

$$\dot{m} = \rho_1 A_1 V_1 = \rho_2 A_2 V_2 = \rho A V = constant \tag{17}$$

For the Conservation of Momentum, we start with the integral form in the x direction from equation 11 and when considering steady flow, $\int_{\mathcal{V}} (\rho u_i)_t dV = 0$. If we view a differential element in this one direction of a stream tube with no frictional forces, we will see Figure 3 [1].

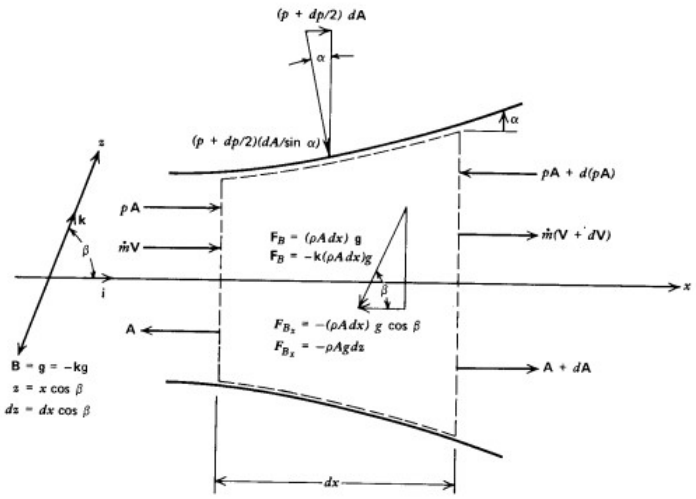

Figure 3: Differential Element of Stream Tube (1D Fluid Flow) [1]

Since we are neglecting frictional forces as stated in the assumptions, we have an inviscid flow resulting in the shear force equaling zero, $F_{shear} = 0$.

$$\int_{\mathcal{V}} \boldsymbol{B_i}\rho \, dV - \int_A pn_i \, d\boldsymbol{A} = \int_A u_i(\rho \boldsymbol{V} \cdot d\boldsymbol{A}) \tag{18}$$

The body forces considered in this problem is gravity which acts in the negative z direction so, in terms of the x direction, equates to $-i\rho Agdz$. The inlet variables of Figure 3 include $p\boldsymbol{A}, \dot{\boldsymbol{m}}\boldsymbol{V}$, and $\boldsymbol{A}$ whereas the outlet across dx results in $p\boldsymbol{A} + d(p\boldsymbol{A}),\ \dot{\boldsymbol{m}}(\boldsymbol{V} + d\boldsymbol{V}),\ \boldsymbol{A} + d\boldsymbol{A}$**.** We also observe that "on the stream tube boundary, the average static pressure intensity is $p + dp/2$, which acts on the area $dA/sin\alpha$" [1]. With the directionality of concern being the x direction, the total boundary surface force is just $\left(p + \frac{dp}{2}\right) dA$. Applying to equation 18 yields

$$-\rho Agdz + pA + \left(p + \frac{dp}{2}\right) dA - pA - d(pA) = \dot{m}(V + dV) - \dot{m}V \tag{19}$$

Simplifying equation 19 and applying equation 17 in the presence of $\dot{m}$ yields the differential form of Bernoulli's equation

$$dp + \rho V dV + \rho g dz = 0 \tag{20}$$

The integrated form can be called the Bernoulli constant

$$\int \frac{dp}{\rho} + \frac{V^2}{2} + gz = constant \tag{21}$$

Both equation 20 and 21 are valid forms of the momentum equation for steady one-dimensional flow of an inviscid fluid [1]. This Momentum equation can be applied to both compressible and incompressible flows, which yields differing results depending on the Mach number. The Mach number is defined as the local velocity divided by the speed of sound of the fluid.

$$M = \frac{V}{a} \tag{22}$$

When the local velocity ratio to the speed of sound is less than one, it is considered to be subsonic, equal to one is sonic, and greater than one is known as supersonic. Using the Mach number in calculations is advantageous since if it is known, then many of the critical parameters such as the critical pressure, density, and temperature can be calculated. Subsonic flows act in a similar manner to incompressible fluids since the changes in the density of the gas is negligible, so we can say that the density is constant, $\rho = constant$ and by integrating the momentum equation 21 becomes the "Bernoulli's equation for the steady frictionless flow of an incompressible fluid" [1]

$$\frac{p}{\rho} + \frac{V^2}{2} + gz = constant \tag{23}$$

As discussed, for sonic or supersonic flow of a compressible fluid, we can express the flow properties by utilizing the Mach number. By rewriting equation 20 and introducing the fact that

body forces are negligible, and that the entropy remains constant with an adiabatic inviscid fluid flow (isentropic flow), we obtain

$$\frac{d\rho}{\rho} + M^2\left(\frac{dV}{V}\right) = 0$$

(24)

Considering the thermodynamics of a one-dimensional steady flow, we will observe the energy balance of the differential fluid element in the stream tube as shown in Figure 4 [1].

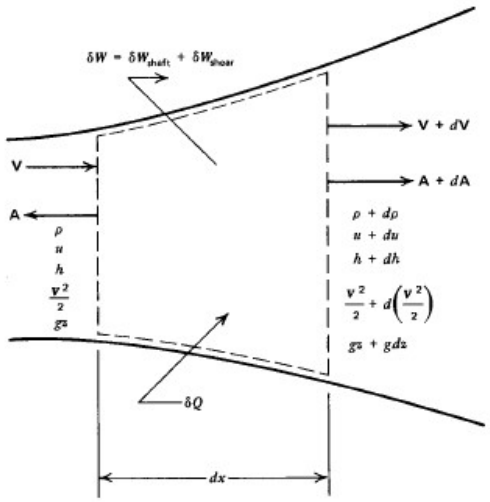

Figure 4: Energy Balance of Differential Fluid Element [1]

Balancing the energy of and applying to the Equation of Energy listed in equation 13, we obtain

$$\delta W - \delta Q + dh + d\left(\frac{V^2}{2}\right) + gdz = 0$$

(25)

Since gases as compressible fluids have small densities, the potential energy term can be neglected, which yields the Energy Equation for a gas to be

$$Q + h_1 + \frac{V_1^2}{2} = W + h_2 + \frac{V_2^2}{2}$$

(26)

We now consider that the flow is adiabatic and has no external work, so $\delta Q = \delta W = 0$. Applying to equation 25 gives the steady adiabatic inviscid compressible fluid flow

$$dh + d\left(\frac{V^2}{2}\right) + gdz = 0$$

(27)

For an isentropic flow, we assume the change in entropy, $ds = 0$ and that since we repeat that we are considering an adiabatic flow, $\delta Q = \delta W = 0$. It is shown that we can relate the changes of entropy, enthalpy, and pressure as [1]

$$t\, ds = dh - vdp = dh - \left(\frac{dp}{p}\right) = 0$$

(28)

Which if plugged into equation 27 yields an energy equation for a steady one-dimensional isentropic flow per unit mass of fluid

$$\frac{dp}{\rho} + d\left(\frac{V^2}{2}\right) + gdz = 0$$

(29)

If we look at the flow of a perfect gas, then we can say that the differential static specific enthalpy, dh, is equal to the specific heat at a constant pressure times the differential static temperature and with the neglect of body forces, equation 27 can be reformed to

$$c_p dt + d\left(\frac{V^2}{2}\right) = 0$$

(30)

If we integrate equation 30 between two states, we find that

$$c_p t + \left(\frac{V^2}{2}\right) = constant$$

(31)

If we desire to introduce the Mach number into these equations, we must introduce relationships of the Mach number variables with the above. It is known that for a perfect gas $c_p = \frac{\gamma R}{\gamma - 1}$ and $a^2 = \gamma R t$, where γ is the specific heat ratio, $\frac{c_p}{c_v}$, and R is the universal gas constant. Introducing these relationships to equation 31 and then implementing the Mach number, $M = \frac{V}{a}$ ultimately yields another form of equation 30, represented with the Mach number [1].

$$\frac{V^2}{2} + \frac{a^2}{\gamma - 1} = constant \tag{32}$$

$$a^2 \left(1 + \frac{\gamma - 1}{2} M^2\right) = constant \tag{33}$$

$$t \left(1 + \frac{\gamma - 1}{2} M^2\right) = constant \tag{34}$$

3.3 Compressible Fluid Flow Critical Conditions

One factor that can have an impact on the flow of a compressible fluid versus an incompressible fluid is the compressibility factor. The compressibility of a fluid will impact many of the thermodynamic properties. The compressibility factor is denoted by F_c and is equal to unity for an incompressible flow. For a compressible flow, the compressibility factor is derived from the equation for the stagnation pressure of a perfect gas with frictionless flow. First defined is the dynamic pressure of the compressible fluid which is related to the equation for the pressure at which the velocity of the flow is zero, also known as the stagnation pressure shown in Equation 35. Equation 36 shows the dynamic pressure of a compressible fluid.

$$\frac{P}{p} = \left(1 + \frac{\gamma - 1}{2} M^2\right)^{\frac{\gamma}{\gamma - 1}} \tag{35}$$

$$q_{comp} = P - p = p\left[\left(1 + \frac{\gamma - 1}{2} M^2\right)^{\frac{\gamma}{\gamma - 1}} - 1\right] \tag{36}$$

If we note that $\frac{\gamma p M^2}{2} = \frac{\rho V^2}{2}$, then we can calculate the compressibility factor to be

$$F_c = \frac{P - p}{\frac{1}{2}\rho V^2} \tag{37}$$

As discussed with the compressibility factor, there can come a point where the velocity reaches zero. For differing parameters that where the speed of the gas is adiabatically decelerated to zero, we call these the stagnation points or conditions. This is called stagnation because the fluid will be stagnant in this state as it will not be moving. The stagnation conditions that can be in the form of temperature, pressure, enthalpy, density, and acoustic speed. Table 1 contains the equations for the stagnation conditions of an isentropic process as defined by Zucrow, M. Gas Dynamics Volume 1, Chapter 3-9 [1].

Stagnation Condition	Equation	
Temperature	$T = t\left(1 + \frac{\gamma - 1}{2} M^2\right)$	(38)
Pressure	$\frac{P}{p} = \left(\frac{T}{t}\right)^{\frac{\gamma}{\gamma-1}} = \left(1 + \frac{\gamma - 1}{2} M^2\right)^{\frac{\gamma}{\gamma-1}}$	(39)
Density	$\frac{\rho_o}{\rho} = \left(1 + \frac{\gamma - 1}{2} M^2\right)^{\frac{1}{\gamma-1}}$	(40)
Enthalpy	$H = (h_2)_{V_2=0} = h + \frac{V^2}{2}$	(41)

Table 1: Stagnation Condition Equations for Isentropic Perfect Gas

From the stagnation condition equations, we can also determine critical conditions. These critical conditions are defined as the conditions that the fluid takes when a gas flow that is subsonic initially flows through a frictionless tube. As the gas expands, the speed of the fluid increases while the temperature and the pressure decrease. The point in the tube where the local speed is equivalent to the acoustic speed is the critical speed of sound which occurs at the sonic condition or $M = 1$. All critical conditions are denoted by an Asterix. It is found that the stagnation acoustic velocity can be represented with the critical speed by

$$a_o^2 = \frac{\gamma + 1}{2} a^{*2} \tag{42}$$

When observing the thermodynamic properties of the fluid at the critical speed of sound, we obtain the critical temperature by setting the local temperature equal to the critical temperature at the sonic condition.

$$t^* = \frac{2}{\gamma + 1} T$$

(43)

By applying $p = \rho RT$ to the stagnation equations of the density and pressure, we obtain the critical values as

$$\frac{p^*}{P} = \left(\frac{t^*}{T}\right)^{\frac{\gamma}{\gamma-1}} = \left(\frac{2}{\gamma + 1}\right)^{\frac{\gamma}{\gamma-1}}$$

(44)

$$\frac{\rho^*}{\rho} = \left(\frac{p^*}{P}\right)^{\left(\frac{1}{\gamma}\right)} = \left(\frac{2}{\gamma + 1}\right)^{\frac{1}{\gamma-1}}$$

(45)

Zucrow [1] shows curves of the critical ratios as a function of the specific heat ratio in Figure 5 below. We should note that at a specific heat ratio of 1.4 which corresponds to gases such as Nitrogen and Air (which are the gases of interest), the critical pressure ratio equals 0.528 or the inverse equates to 1.9.

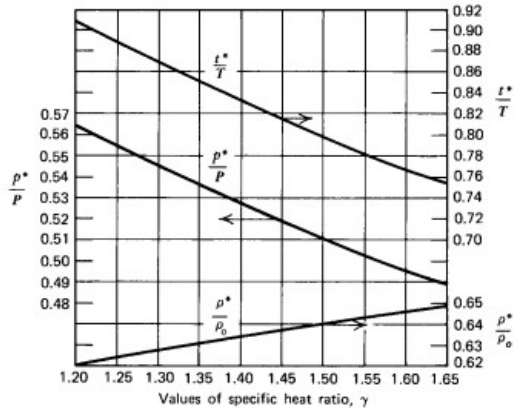

Figure 5: Critical Ratios as a Function of Specific Heat Ratio

For the problem at hand, we will be measuring the mass flow through the orifice. The inlet conditions and geometry of the flow area will be known. It is desirable to compare the discharge coefficient for the theoretical versus the experimental. To interpret the mass flow, we can use the continuity equation for a perfect gas crossing a flow area and apply the acoustic speed of sound and Mach number. We know from equation 17 the continuity of mass equation and also that $a = \sqrt{\gamma R t}$ and $M = V/a$.

$$\dot{m} = \frac{ApV}{Rt} = \frac{ApV}{\sqrt{\gamma Rt}}\left(\sqrt{\frac{\gamma}{Rt}}\right) = ApM\left(\sqrt{\frac{\gamma}{Rt}}\right) = constant \tag{46}$$

Considering equation 38, we can express the mass flow shown in equation 46 in terms of the stagnation temperature

$$\dot{m} = ApM\left[\frac{\gamma}{RT}\left(1 + \frac{\gamma - 1}{2}M^2\right)^{\frac{1}{2}}\right] = constant \tag{47}$$

Similarly, we can express the mass flow in terms of the stagnation pressure shown in equation 39 which becomes

$$\dot{m} = APM\left(\frac{\gamma}{RT}\right)^{\frac{1}{2}}\left(1 + \frac{\gamma - 1}{2}M^2\right)^{-\frac{\gamma+1}{2(\gamma-1)}} = constant \tag{48}$$

As with the pressure, density, and temperature, we also can define a critical mass flow when the speed of the gas is equal to the critical speed of sound. The critical mass flow will be the maximum flow rate that is achieved when the gas reaches the critical speed of sound. This parameter will

also depend on the area that the flow is moving through or the critical area ratio which is defined by the local area over the critical area in the passage.

$$\frac{A}{A^*} = \frac{1}{M}\left[\frac{2}{\gamma+1}\left(1+\frac{\gamma-1}{2}M^2\right)\right]^{\frac{\gamma+1}{2(\gamma-1)}} \tag{49}$$

It then follows from equation 48 that

$$\dot{m} = AP\left(\frac{\gamma}{RT}\right)^{\frac{1}{2}}\left(\frac{2}{\gamma+1}\right)^{-\frac{\gamma+1}{2(\gamma-1)}}\left(\frac{1}{\frac{A}{A^*}}\right) \tag{50}$$

If we apply this mass flow rate at the sonic condition, then the critical mass flow rate is

$$\dot{m}^* = PA^*\left(\frac{\gamma}{RT}\right)^{\frac{1}{2}}\left(\frac{2}{\gamma+1}\right)^{-\frac{\gamma+1}{2(\gamma-1)}} \tag{51}$$

Or

$$\dot{m}^* = \frac{PA^*}{\sqrt{\frac{\gamma}{RT}}}\gamma\left(\frac{2}{\gamma+1}\right)^{-\frac{\gamma+1}{2(\gamma-1)}} \tag{52}$$

3.4 Compressible Flow in the Presence of an Area Change

The study of compressible fluid flow in the presence of an area change is important to fully understanding the flow through a sharp edge orifice. Experimentally, the flow will be entering a chamber with an approximate diameter of Ø 0.150 and a 0.0007" hole, so the area change will be a magnitude of over one-hundred. The area change will allow us to understand the impact on the expansion and compression of the flow depending on the inlet conditions (i.e. subsonic or supersonic).

First, we define a couple of terms; nozzle and diffuser. A nozzle is a device that increases the velocity of a fluid while decreasing the pressure. A diffuser is a device that does the exact opposite of a nozzle, where the pressure increases while slowing down the velocity. It can be shown that if a flow entering a passage is subsonic ($M < 1$), then to yield nozzle action, the passage must converge while for nozzle action to occur with a supersonic flow ($M > 1$), then the passage much diverge. The opposite it true for a diffuser.

Then we have the condition of choked flow where a diverging passage will decelerate an entering subsonic flow toward a zero velocity to become more subsonic, while accelerating a supersonic flow toward the max isentropic speed. When a converging passage is present, an entering subsonic flow will accelerate toward the sonic speed and decelerate a supersonic flow toward the sonic speed. What is seen is that when the flow reaches the sonic speed in a converging passage, the area reaches a minimum where the flow is said to be choked. When there is a diverging passage, the Mach number will depend on the downstream boundary conditions. This can be related to the

pressure downstream of the orifice as seen in Figure 6, which is representative of the orifice being explored.

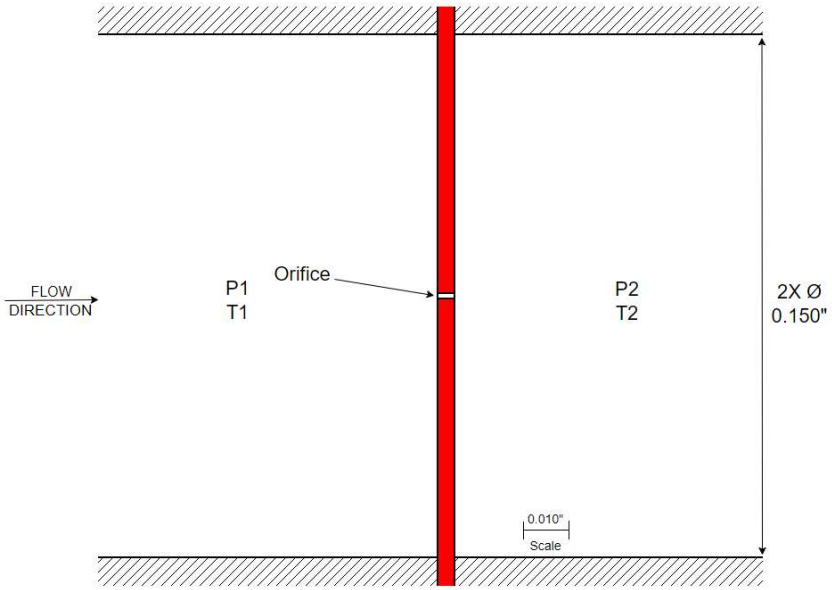

Figure 6: Orifice Plate Cross Section View of Area Change

When a passage goes from converging to diverging, the smallest area is considered the throat and is where the flow reaches its critical points. With the passage starting off converging and then going diverging, it is found that the downstream conditions will have an impact on the flow. Since we are concerned with the mass flow of the orifice in the subsonic, sonic, and supersonic regions, we will explore the impact of the downstream pressure on the mass flow when in this critical area.

It has been shown that when the mass flow enters the throat, and the backpressure can have an impact when in the subsonic flow conditions. This is due to disturbances in the pressure that is felt, and the fluid creates a jet stream. When the fluid reaches sonic speed conditions, the critical mass flow rate is achieved and become independent of the downstream pressure. This is referred to as

the Rule of Forbidden Signals [4], which states, that the effect of pressure changes produced by a body moving at a speed faster than the speed of sound cannot reach points ahead of the body (von Kármán, Jour. Aero. Sci., Vol. 14, No. 7 (1947)). The body in our case is static, but the flow velocity reaches the speed of sound. With a downstream pressure that forces the flow to become sonic or reach a Mach number of unity, a change in the backpressure can't reach points upstream of the throat.

3.5 Flow Through and Orifice Plate and Resulting Restriction

Similar to the derivation of the mass flow in the subsonic and sonic region (non-critical and critical points) with guidance of Zucrow [1], we can look at an orifice plate as the change in area of a passage that will converge to the throat and then diverge. It is desirable to simplify the mass flow even more and relate it to the restriction of the orifice. When studying a thin orifice plate, such as described in the assumptions, we have seen the critical pressure ratio equal around 0.53 on average depending on the specific heat ratio of the gas being tested.

As shown in Mark's Standard Handbook for Mechanical Engineers [2], if we section passage into three, where the upstream section is section 1, the orifice is section 2, and the downstream section is section 3, then we can observe that the energy balance in these sections equates to

$$\frac{(\bar{v}_2^2 - \bar{v}_1^2)}{2g} = -h_{12} \tag{53}$$

Where g, refers to the body force of gravity and h is the entropy. It is further shown that if the velocity at the orifice (section 2) when flowing a gas can be described using the coefficient of

discharge, C_d which refers to the ratio of the experimental volumetric flow to the ideal volumetric flow, $Q_{experimental}\ and\ Q_{ideal}$.

$$C_d = \frac{\dot{m}}{A\sqrt{2\rho\Delta P}} = \frac{Q_{experimental}}{Q_{ideal}} \tag{54}$$

$$\bar{v}_2 = \frac{\left(C_d\sqrt{2g(h_1 - h_2)}\right)}{\sqrt{1 - \left(\frac{A_2}{A_1}\right)^2\left(\frac{v_1}{v_2}\right)^2}} \tag{55}$$

With an adiabatic reversible flow of an ideal gas, it follows from above that the velocity becomes

$$\bar{v}_2 = C_d \frac{\left(\sqrt{2gP_1\bar{v}_1\left(\frac{\gamma}{\gamma-1}\right)\left[1 - \left(\frac{P_2}{P_1}\right)^{\frac{\gamma-1}{\gamma}}\right.}\right)}{\sqrt{1 - \left(\frac{A_2}{A_1}\right)^2\left(\frac{P_2}{P_1}\right)^{\frac{2}{\gamma}}}} \tag{56}$$

And the mass flow rate after rearranging from above can be described as

$$m = C_d A_2 P_2 \frac{\left(\sqrt{\frac{2g}{RT}\left(\frac{\gamma}{\gamma-1}\right)\left(\frac{P_1}{P_2}\right)^{\frac{\gamma-1}{\gamma}}\left[\left(\frac{P_1}{P_2}\right)^{\frac{\gamma-1}{\gamma}} - 1\right]}\right)}{\sqrt{1 - \left(\frac{A_2}{A_1}\right)^2\left(\frac{P_2}{P_1}\right)^{\frac{2}{\gamma}}}} \tag{57}$$

Equation 57 is true for subsonic flow conditions for the 1D steady state adiabatic isentropic flow of an ideal gas. Since we know that a sonic flow condition will occur when the pressure ratio is

approximately $\frac{P_1}{P2} \geq 1.9\ or\ \frac{P_2}{P_1} \leq 0.53$ and that the downstream pressure has no impact on the mass flow, then

$$m = C_d A_2 P_1 \sqrt{\frac{g}{RT}\gamma\left(\frac{2}{\gamma+1}\right)^{\frac{\gamma+1}{\gamma-1}}} \tag{58}$$

3.6 Orifice Edge Conditions and Pressure Ratio vs Theoretical Flow Rate

One interest is to represent the flow in volumetric flow and to use a representation of equivalent restriction for the mass flow based on the coefficient of discharge and the area of the orifice. From Mark's Standard Handbook for Engineers, it is said that the edge condition of an orifice can determine its' coefficient of discharge and follows Figure 7 [2].

Type	Coefficient		
	C	C_c	C_v
Sharp-edged orifice	0.61	0.62	0.98
Rounded-edged orifice	0.98	1.00	0.98
Short tube, $\frac{L}{D} \sim 1$	0.80	1.00	0.80
Borda	0.51	0.52	0.98

Figure 7: Coefficient of Discharge of Orifice Edge Conditions [2]

Since we are interested in a sharp edge orifice, we would theoretically expect $C_d = 0.61$. With the 0.0007" hole size target, the theoretical "sharp edge" potentially not perfect and may take more of a rounded edge shape which would lead to a $C_d = 0.98$. Once experimental data is taken, the edge type will reveal itself better.

To make equations 57 and 58 easier to work with and result in a given restriction, we can first define the resistance by the coefficient of discharge and the area starting with the conservation of energy producing Bernoulli's equation and the orifice plate sections. Rearranging equation 23 and applying to the orifice sections

$$\frac{P_1}{\rho} = \frac{V_2^2}{2g} + \frac{P_2}{\rho} \tag{59}$$

$$V_2 = \sqrt{\frac{2g\ (P_1 - P_2)}{\rho}} \tag{60}$$

We know that

$$Q\ (Volumetric\ Flow\ Rate) = A_2 V_2 \tag{61}$$

And

$$A_2 = C_d A \tag{62}$$

So

$$Q = C_d A \sqrt{\frac{2g\ (P_1 - P_2)}{\rho}} \tag{63}$$

If

$$Q\left(\frac{ft^3}{s}\right) = I\ (gpm) * 0.1337/60 \tag{64}$$

$$A(ft^2) = A(in^2) * \frac{1}{144} \tag{65}$$

$$g = 32.16\frac{ft}{s^2} \tag{66}$$

$$\rho\left(\frac{lb_m}{ft^3}\right) = Specific\ Gravity\ x\ 62.43 \tag{67}$$

$$P\left(\frac{lb_f}{ft^2}\right) = P\left(\frac{lb_f}{in^2}\right) * 144 \tag{68}$$

Then

$$I = \frac{60C_dA}{0.1337 * 144}\sqrt{\frac{2 * 32.16 * 144\ (P_1 - P_2)}{62.43 * S}} \tag{69}$$

$$I = 20 * 1.898 * C_dA\sqrt{\frac{(P_1 - P_2)}{S}} \tag{70}$$

If

$$\Omega\ (Flow\ Resitance) = \frac{1}{1.898 * C_dA} \tag{71}$$

$$\Omega\ (Flow\ Resitance) = \frac{.5268}{C_dA}\ \ OR\ C_dA = \frac{0.5268}{\Omega} \tag{72}$$

Then

$$I = \frac{20}{\Omega}\sqrt{\frac{(P_1 - P_2)}{S}} \tag{73}$$

Or

$$\Omega = \frac{20}{I}\sqrt{\frac{(P_1 - P_2)}{S}} \tag{74}$$

This describes the resistance to fluid flow which follows laws described by [5]. To apply this to gas flow, we can use equations 57 and 58 for both sonic and subsonic conditions. Starting with sonic conditions we rearrange to get

$$m = \left(\frac{AP_1}{\sqrt{T_1}}\right)\sqrt{\left(\frac{\gamma g}{R}\right)\left(\frac{2}{\gamma + 1}\right)^{\frac{\gamma+1}{\gamma-1}}} \tag{75}$$

Where standard conditions here are defined as 59°F and 1 atmosphere (14.7 psia) and

$m = Mass\ Flow\ Rate\ \left(\frac{lb_m}{s}\right)$

$A = Effective\ Area = C_d A$

$T = Temperature\ (°R)$

$R = Gas\ Constant\ \left(\frac{(ft*lb_f)}{lb_m*°R}\right)$

$C_d = Coefficient\ of\ Discharge$

$\gamma = Specific\ Heat\ Ratio$

$g = Gravity\ \left(32.17\frac{ft}{s^2}\right)$

We have the known relationships of

$$\Omega\,(Flow\ Resitance) = \frac{.5268}{C_d A}\ \ OR\ C_d A = \frac{0.5268}{\Omega} \tag{76}$$

And the equation of state of a perfect gas as

$$PV = MRT\ or\ V = \frac{MRT}{P} \tag{77}$$

The flow at the standard conditions listed above is

$$I = (SCFM) = \frac{RT_s}{P_s} m * \left[\frac{60sec}{\min}\right]\left[\frac{1ft}{12in}\right]^2 = \frac{60RT_s}{144P_s} m \tag{78}$$

Combining our knowns from equation 76 and 78 into equation 75 we get

$$\frac{I(144)P_s}{60RT_s} = \frac{0.5268P_1}{\Omega\sqrt{T_1}}\left[\frac{\gamma g}{R}\left(\frac{2}{\gamma+1}\right)^{\frac{\gamma+1}{\gamma-1}}\right]^{\frac{1}{2}} \tag{79}$$

$$\Omega = \frac{0.5268P_1(60)RT_s}{\sqrt{T_1}I(144)P_s}\sqrt{g}\left[\frac{\gamma}{R}\left(\frac{2}{\gamma+1}\right)^{\frac{\gamma+1}{\gamma-1}}\right]^{\frac{1}{2}}$$

$$= \frac{\left(0.5268 * 60 * 518.67°R * \sqrt{32.17}\right)}{144 * 14.7\ psi}\left[\frac{P_1}{I\sqrt{T_1}}\right]\left[\gamma R\left(\frac{2}{\gamma+1}\right)^{\frac{\gamma+1}{\gamma-1}}\right]^{\frac{1}{2}} \tag{80}$$

$$\Omega = 43.927\left[\frac{P_1}{I\sqrt{T_1}}\right]\left[\gamma R\left(\frac{2}{\gamma+1}\right)^{\frac{\gamma+1}{\gamma-1}}\right]^{\frac{1}{2}} \tag{81}$$

If we let

$$B = 43.927\left[\gamma R\left(\frac{2}{\gamma+1}\right)^{\frac{\gamma+1}{\gamma-1}}\right]^{\frac{1}{2}} \tag{82}$$

And let

$$C = \frac{B}{\sqrt{T_s}} \tag{83}$$

$$T_f = \sqrt{\frac{530}{T(°F)+460}} \tag{84}$$

Then

$$I = \frac{CP_1T_f}{\Omega} = \frac{CP_1T_f}{\frac{.5268}{C_dA}} = \frac{C_dACP_1T_f}{0.5268} \tag{85}$$

When using pressure units of psia and volumetric flow units of SCCM, $C = 276000$. If we assume for an orifice diameter of 0.0007" that $P_1 = 100\ psia$, $\gamma = 1.4\ for\ N_2$, and $T = 70°F$, then the theoretical volumetric flow rate in the sonic region, $\frac{P_1}{P_2} \geq 1.9$ with a sharp edge and rounded edge orifice equates to the values shown in Table 2

Orifice Edge Type	Coefficient of Discharge	Volumetric Flow (SCCM)
Sharp	0.61	12.30
Rounded	0.98	19.76

Table 2: Theoretical Volumetric Flow Rate of Orifice with Sharp and Rounded Edge Condition

When considering a subsonic flow, the mass flow will depend more on the downstream conditions, in this case the backpressure. To evaluate the flow in these conditions, we start by rearranging equation 57

$$m = \left(\frac{AP_1}{\sqrt{T_1}}\right)\left[\left(\frac{2\gamma g}{(\gamma-1)R}\right)\left[\left(\frac{P_2}{P_1}\right)^{\frac{2}{\gamma}} - \left(\frac{P_2}{P_1}\right)^{\left(\frac{\gamma+1}{\gamma}\right)}\right]\right]^{\frac{1}{2}} \tag{86}$$

Inserting equation 76 and 78 this time into equation 84 will follow

$$\frac{I(144)P_s}{60RT_s} = \frac{0.5268P_1}{\Omega\sqrt{T_1}}\left[\left(\frac{2\gamma g}{(\gamma-1)R}\right)\left[\left(\frac{P_2}{P_1}\right)^{\frac{2}{\gamma}} - \left(\frac{P_2}{P_1}\right)^{\left(\frac{\gamma+1}{\gamma}\right)}\right]\right]^{\frac{1}{2}} \tag{87}$$

$$\Omega = \frac{0.5268P_1(60)RT_s}{\sqrt{T_1}I(144)P_s}\sqrt{2g}\left[\left(\frac{\gamma}{(\gamma-1)R}\right)\left[\left(\frac{P_2}{P_1}\right)^{\frac{2}{\gamma}} - \left(\frac{P_2}{P_1}\right)^{\left(\frac{\gamma+1}{\gamma}\right)}\right]\right]^{\frac{1}{2}}$$

$$= 62.16\frac{P_1}{\sqrt{T_1}I}\left[\left(\frac{\gamma R}{(\gamma-1)}\right)\left[\left(\frac{P_2}{P_1}\right)^{\frac{2}{\gamma}} - \left(\frac{P_2}{P_1}\right)^{\left(\frac{\gamma+1}{\gamma}\right)}\right]\right]^{\frac{1}{2}} \tag{88}$$

$$\mathrm{I} = \frac{CFP_1C_dA}{0.5268} \tag{89}$$

Where

$$F = \frac{62.16}{43.927}\sqrt{\frac{\left[\left(\frac{P_2}{P_1}\right)^{\frac{2}{\gamma}} - \left(\frac{P_2}{P_1}\right)^{\left(\frac{\gamma+1}{\gamma}\right)}\right]}{(\gamma-1)\left(\frac{2}{\gamma+1}\right)^{\frac{\gamma+1}{\gamma-1}}}} = 1.415\sqrt{\frac{\left[\left(\frac{P_2}{P_1}\right)^{\frac{2}{\gamma}} - \left(\frac{P_2}{P_1}\right)^{\left(\frac{\gamma+1}{\gamma}\right)}\right]}{(\gamma-1)\left(\frac{2}{\gamma+1}\right)^{\frac{\gamma+1}{\gamma-1}}}} \tag{90}$$

Equation 87 follows similarly to the flow described in [5] technical hydraulic handbook.

Again, when using pressure units of psia and volumetric flow units of SCCM, $C = 276000$. If we assume for an orifice diameter of 0.0007" that $P_1 = 100\ psia$, $\gamma = 1.4\ for\ N_2$, $T = 70°F$, and $P2$ takes the values as shown in the table, then the theoretical volumetric flow rate in the subsonic region, $\frac{P_1}{P_2} < 1.9$ with a sharp edge and rounded edge orifice equates to the values shown in Table 3 and 4.

P1	P2	Pressure Ratio	Volumetric Flow (SCCM)
100	90	1.1	7.60
	80	1.3	10.08
	70	1.4	11.47
	60	1.7	12.17

Table 3: Sharp Edge Orifice Cd Volumetric Flow Rate (.0007" Orifice)

P1	P2	Pressure Ratio	Volumetric Flow (SCCM)
100	90	1.1	12.20
	80	1.3	16.19
	70	1.4	18.43
	60	1.7	19.55

Table 4: Rounded Edge Orifice Cd Volumetric Flow Rate (.0007" Orifice)

The pressure ratio vs theoretical volumetric flow rate curve for the sharp and rounded edge conditions of a 0.0007” orifice takes the shape shown in Figure 8. The boundary for the Sonic to Subsonic Regions are split by the red vertical line, where the right side is the sonic region, and the left side is the subsonic region.

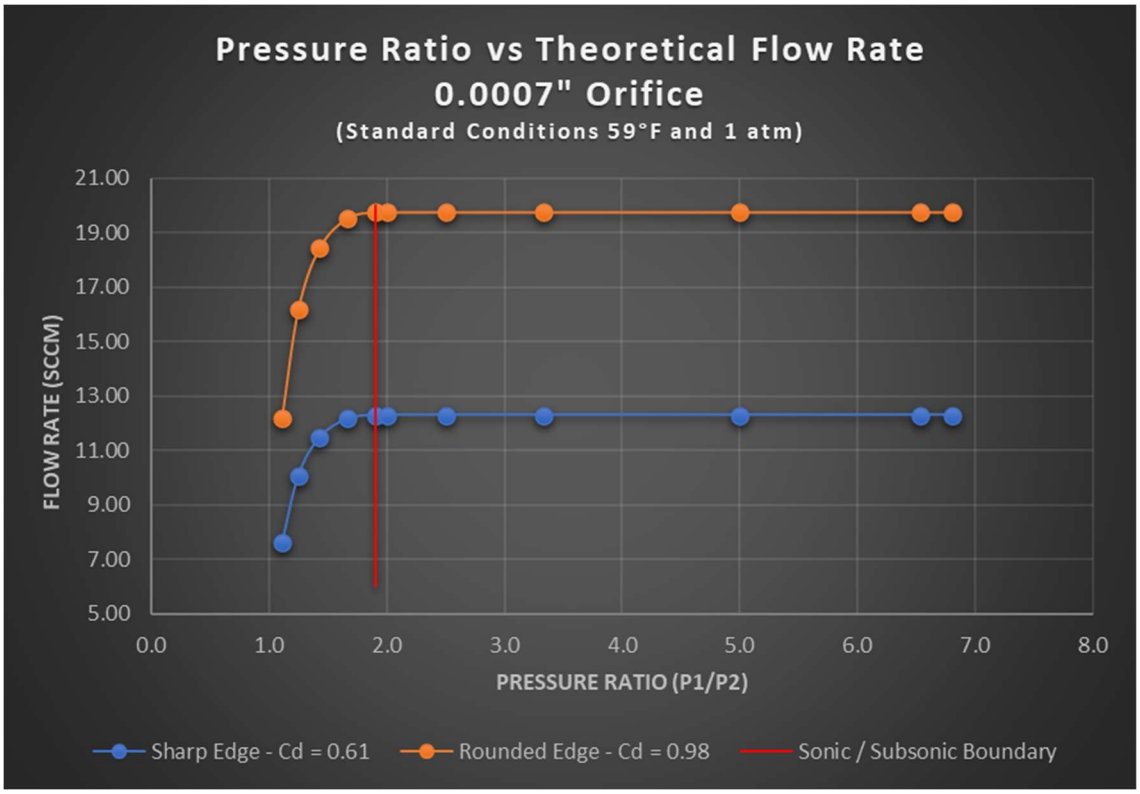

Figure 8: Pressure Ratio vs Theoretical Flow Rate (0.0007" Orifice)

We can see from the theoretical calculations that in the sonic region, the flow rate remains constant. It is not until a pressure ratio smaller than 1.9 where the flow rate changes since the backpressure starts having an impact on the fluid which follows from the theoretical derivations and research.

3.7 Laser Drilling and Measurement of a Single Orifice

An orifice was produced on a proprietary laser in a 0.005” stainless steel plate. Exploration of the parameters were used to discover the smallest hole that we could produce, which resulted in a 0.0007” hole, measured using a proprietary vision system. Below are pictures of the orifice, and the methods used to measure it.

The first image shown in Figure 9 is taken at 20X and the orifice is very hard to see, so Figure 10 is zoomed in to 500X to get a clearer image. We can see the ablated hole with a burn mark. From inspection, the hole seems to be fairly round and sharp.

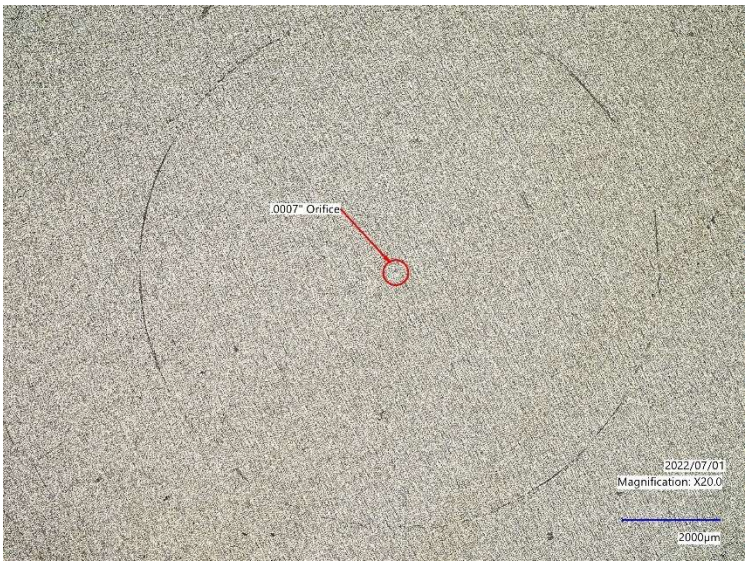

Figure 9: Laser Drilled Orifice, 200X

Figure 10: Laser Drilled Orifice, 500X

A further magnification was used to try and obtain the most accurate measurement possible, which was achieved at 2500X (the maximum magnification that the vision system is capable of). From the measurement in Figure 11, we can see that the hole measure 0.0006958 inches in diameter but does not appear to be perfectly round.

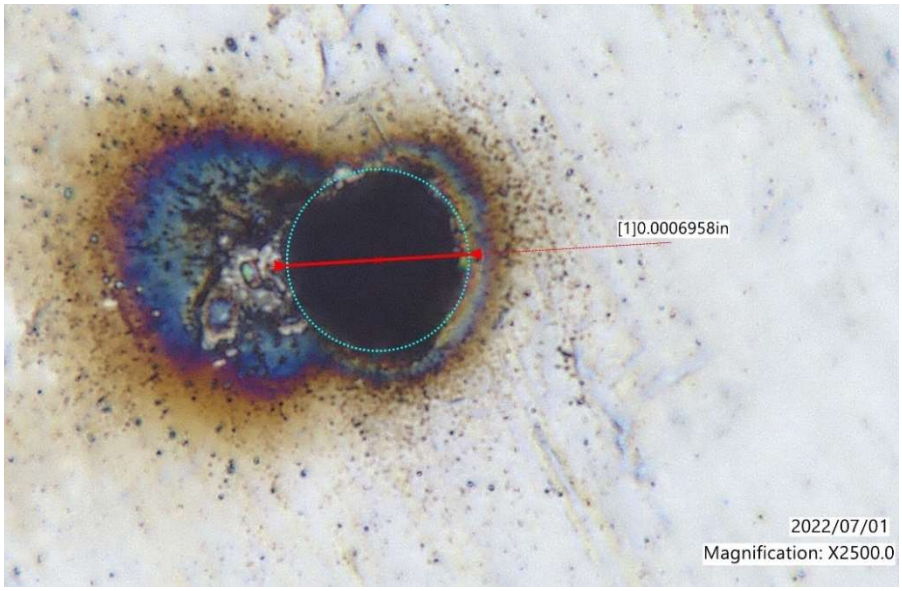

Figure 11: Laser Drilled Hole, 2500X, with Measurement

An attempt was made to get a clearer picture by playing with the lighting and surface features in the vision system. Figure 12 shows the orifice with a min and max hole diameter. The shape is also more visible. The min diameter measured is 0.000607” while the largest is 0.000746”. The orifice looks to take a sort of triangular shape.

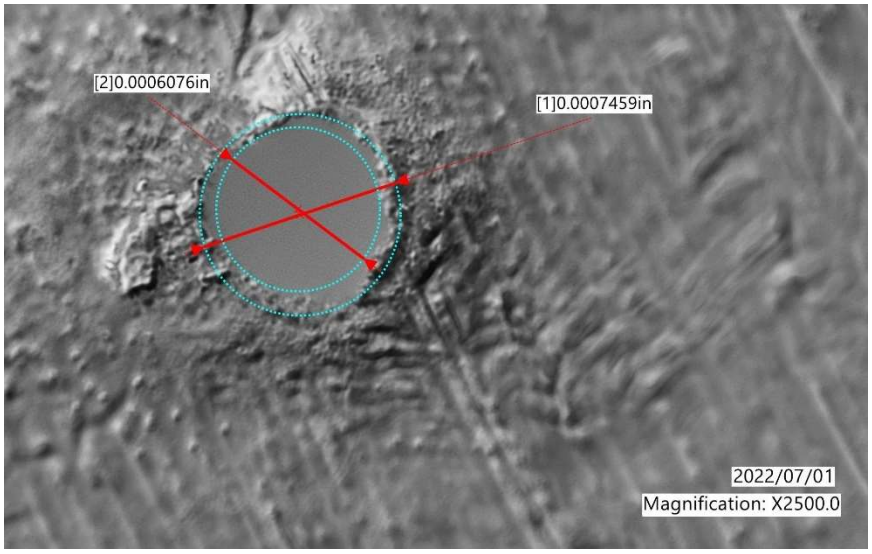

Figure 12: Laser Drilled Hole: Surface Texture with Min / Max Diameter

Diving further into the hole measurement, we used a 3D depth analysis to see the shape rather than relying on the 2D image.

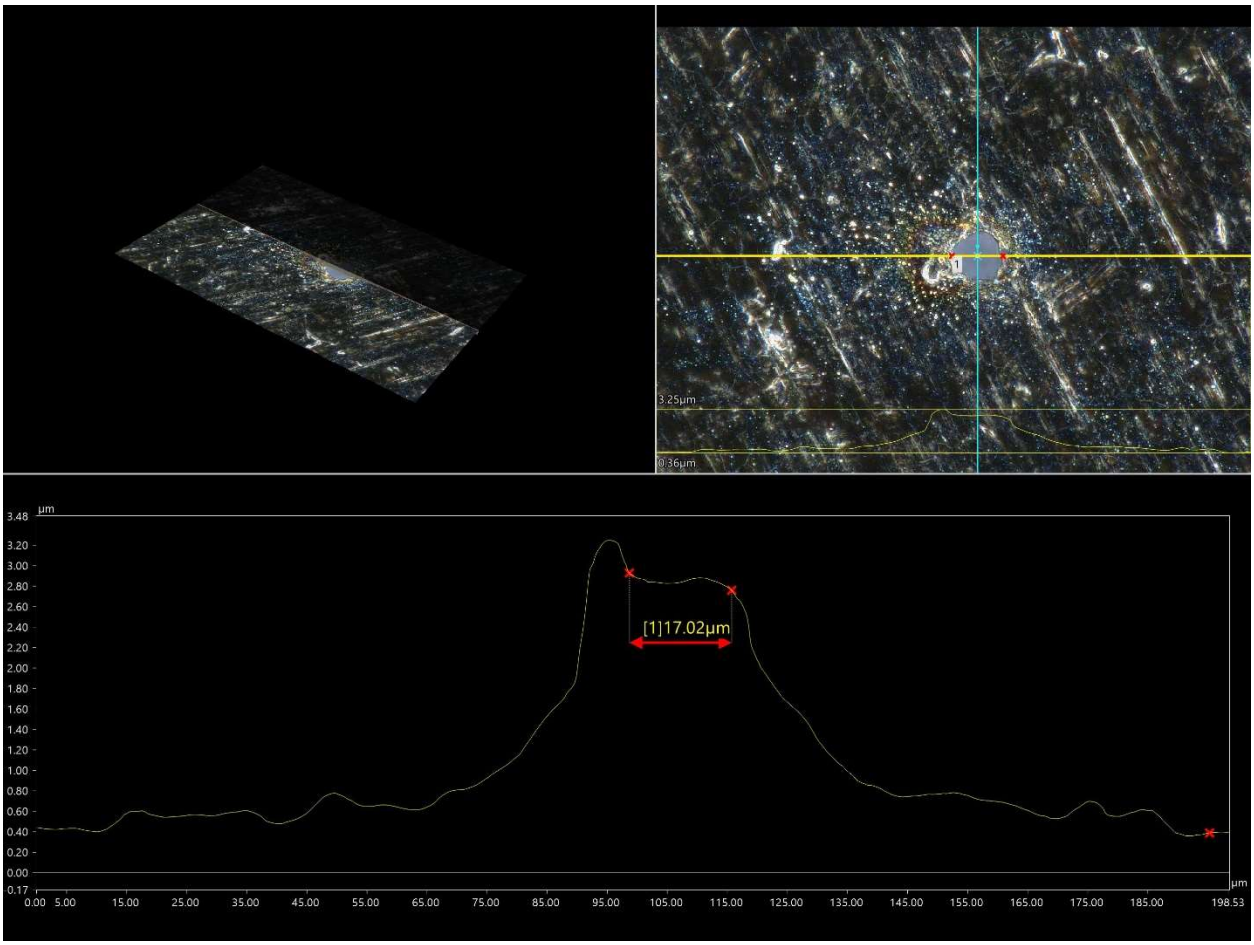

Figure 13: Laser Drilled Hole 3D Depth Composition

Figure 13 shows the profile of the hole and the measurement taken in the horizontal plane. We can see a dip of the left side of the orifice, which looks to be some deformation at the burn site. The hole also looks to be slightly tapered but will be flowed in the direction to catch the sharper edge of the orifice.

3.8 Pressure Ratio vs Experimental Flow Rate of the Laser Drilled Orifice

The flow test was set up with a 99.9% purity Nitrogen gas. The schematic used to set up the test is shown below in Figure 14 where the upstream and downstream pressures of the orifice were monitored. Before testing occurred, a thorough leak test was completed to ensure the most accurate results possible. The pressure gages and the flow meter have an accuracy of 0.5% of reading to ensure the highest accuracy results possible for such a highly restrictive orifice.

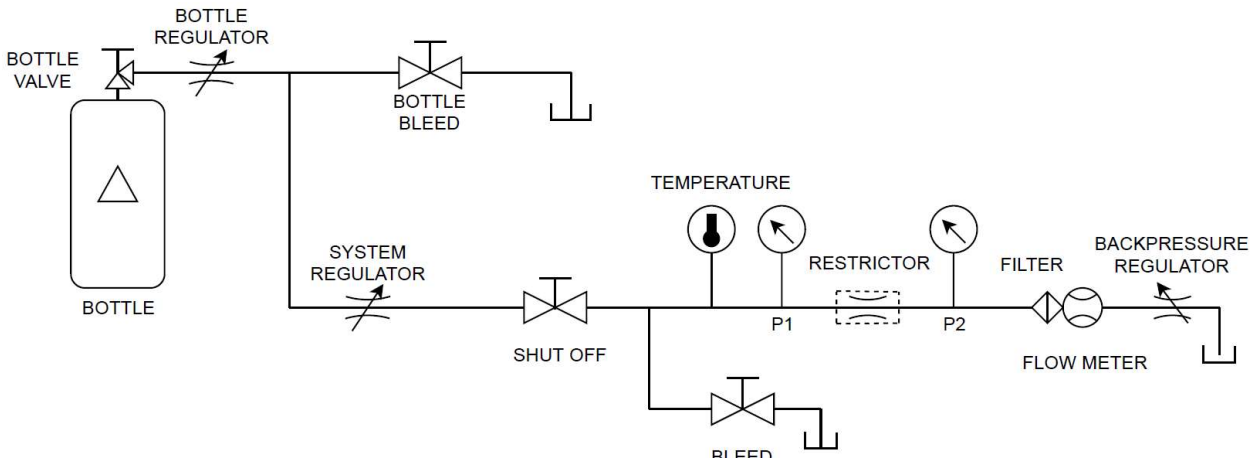

Figure 14: Gas Flow Test Experimental Schematic

As described in the theoretical section, a 100 psia constant upstream pressure was applied, while the backpressure was varied to hit many different pressure ratios varying by 10 psia, though 50 psia was not included as a pressure ratio of 1.9 (sonic boundary) was desired, so 52.65 was utilized. There is no flow directly to atmosphere as the flowmeter induces some backpressure to the setup, resulting in the lowest downstream pressure of 15.3 psia (though during the test, atmosphere was measured at 14.78 psia). The flow test results can be found in Table 5.

Pressure Ratio (P1/P2)	Pressure Ratio (P2/P1)	Pressure (PSIA)		Flow	Test Temperature
		P1	P2	SCCM	°F
6.56	0.153	100.3	15.3	13.19	70.1
5.00	0.200	100	20	13.16	70.2
3.33	0.301	99.8	30	13.13	70.2
2.49	0.402	99.8	40.1	13.07	70.2
1.90	0.527	100	52.65	12.833	70.4
1.66	0.601	99.9	60.06	12.449	70.6
1.42	0.702	99.9	70.12	11.64	70.6
1.25	0.801	99.9	80	9.88	70.7

Table 5: Experimental Pressure Sweep Results (0.0007” Orifice)

Figure 15 is used as a graphical representation of Table 5.

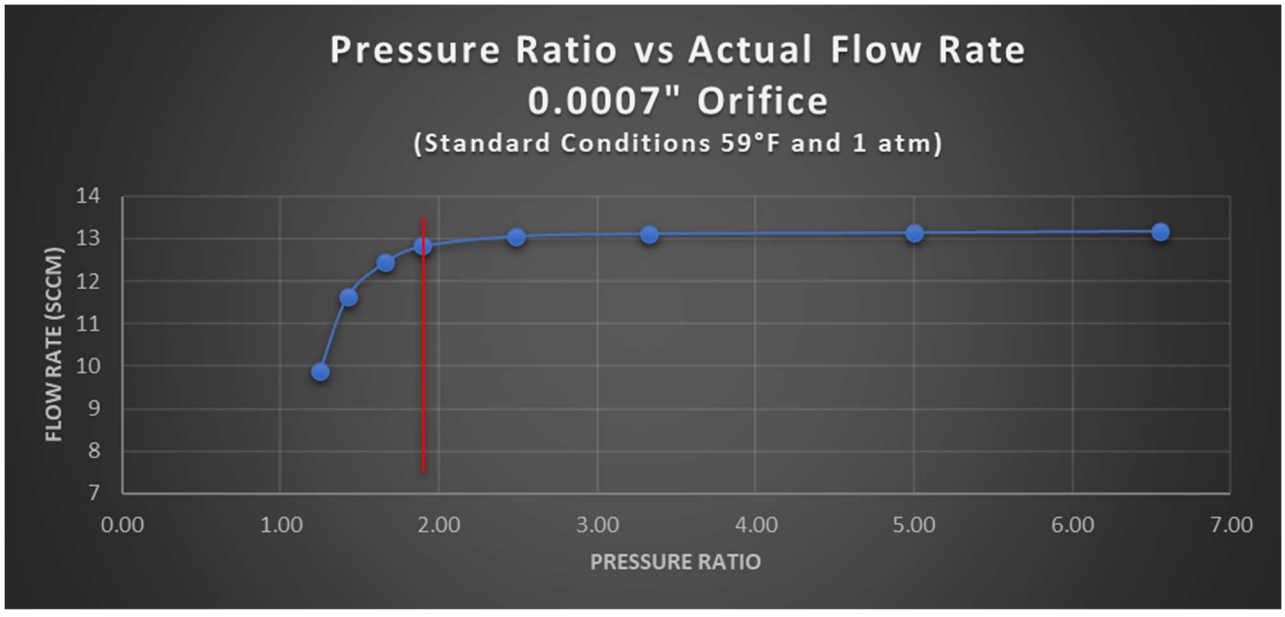

Figure 15: Experimental Pressure Sweep of 0.0007" Orifice

We can see that the shape of the curve agrees well with the theoretical curves shown in Figure 8, but from Figure 15 and Table 5, we can see that in the "sonic" region, the flow rate is not completely constant and deviates before the pressure ratio of 1.9.

The flow rates can also be seen to match better with coefficient of discharge of a sharp edge orifice listed at 0.61. Plotting the actual flow with the theoretical flows can be seen in Figure 16. A closer look at the actual vs the theoretical sharp edge orifice can be seen in Figure 17.

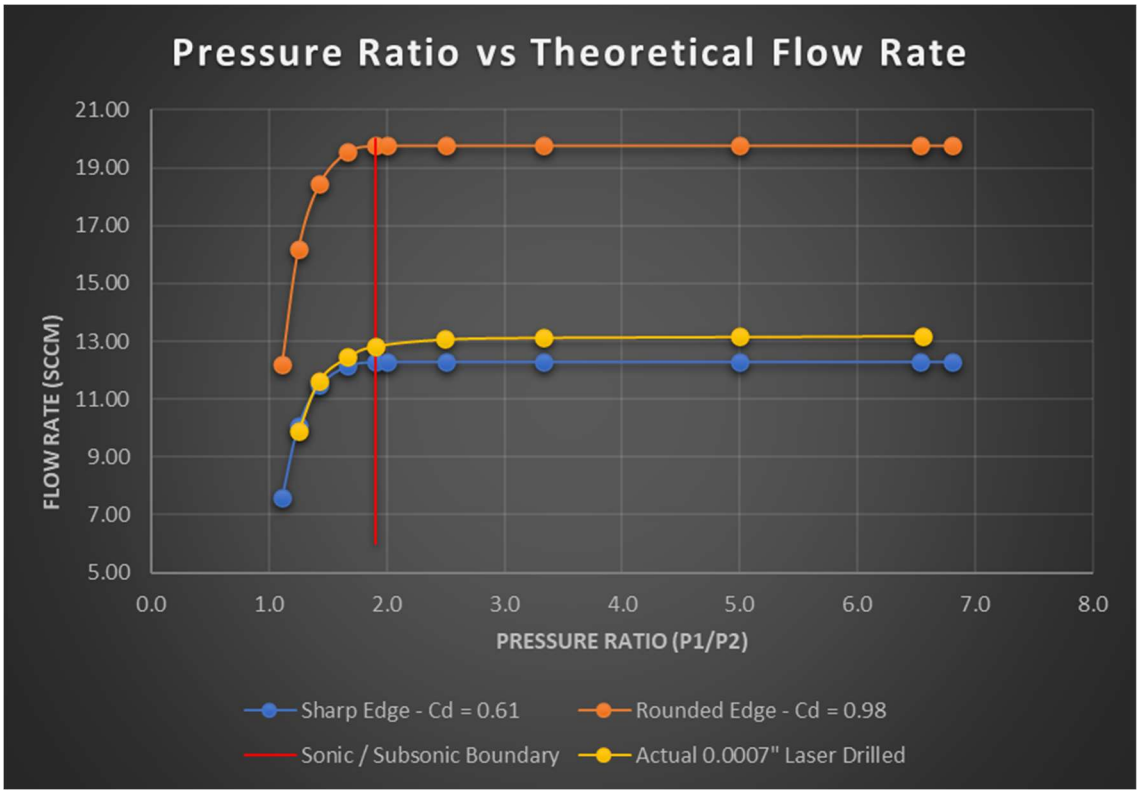

Figure 16: Theoretical vs Experimental Pressure Ratio vs Flow Rate (0.0007" Orifice)

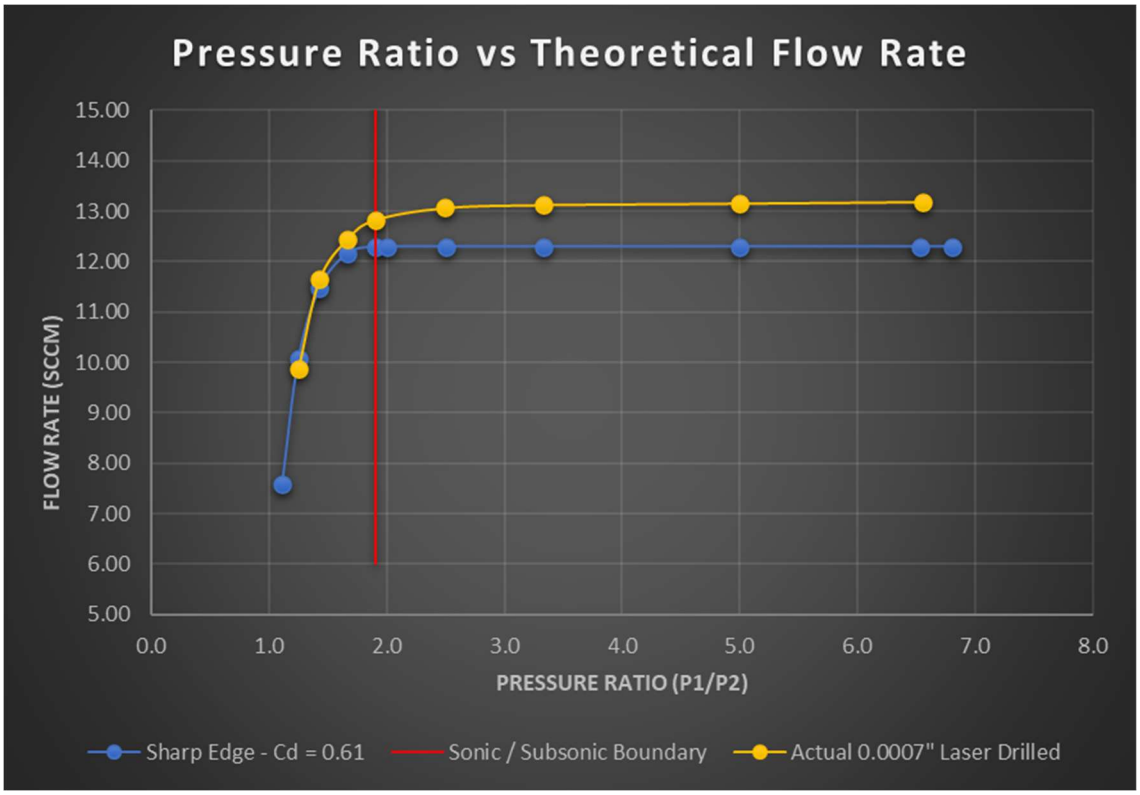

Figure 17: Experimental vs Theoretical Orifice Pressure Ratio vs Theoretical Flow Rate

Assessing the percent difference at similar pressure ratios of the actual vs the theoretical discharge coefficients, we find that the subsonic region has a minimum of 1.45% and a maximum of 2.3% whereas the sonic region is much different at a minimum of 4.25% at the sonic boundary and a maximum in the sonic region of 6.99% as seen in Table 6.

% Difference	Region
1.97	Subsonic
1.45	
2.30	
4.25	Sonic
6.08	
6.53	
6.76	
6.99	

Table 6: Percent Difference of Experimental vs Theoretical Sharp Edge Curve

If we use a coefficient of discharge of 0.65, in the theoretical calculations, the percent difference is much better in the sonic region max of 2.1% at the sonic boundary of 1.9 and under 0.64% for the rest of the sonic region, but the subsonic region then suffers with a maximum of 8.32% and a minimum of 4.05% as shown in Table 7 and Figure 18.

% Difference	Region
8.32	Subsonic
4.90	
4.05	
2.10	Sonic
0.27	
0.18	
0.41	
0.64	

Table 7: Percent Difference when Applying 0.65 Discharge Coefficient to Theoretical Curve

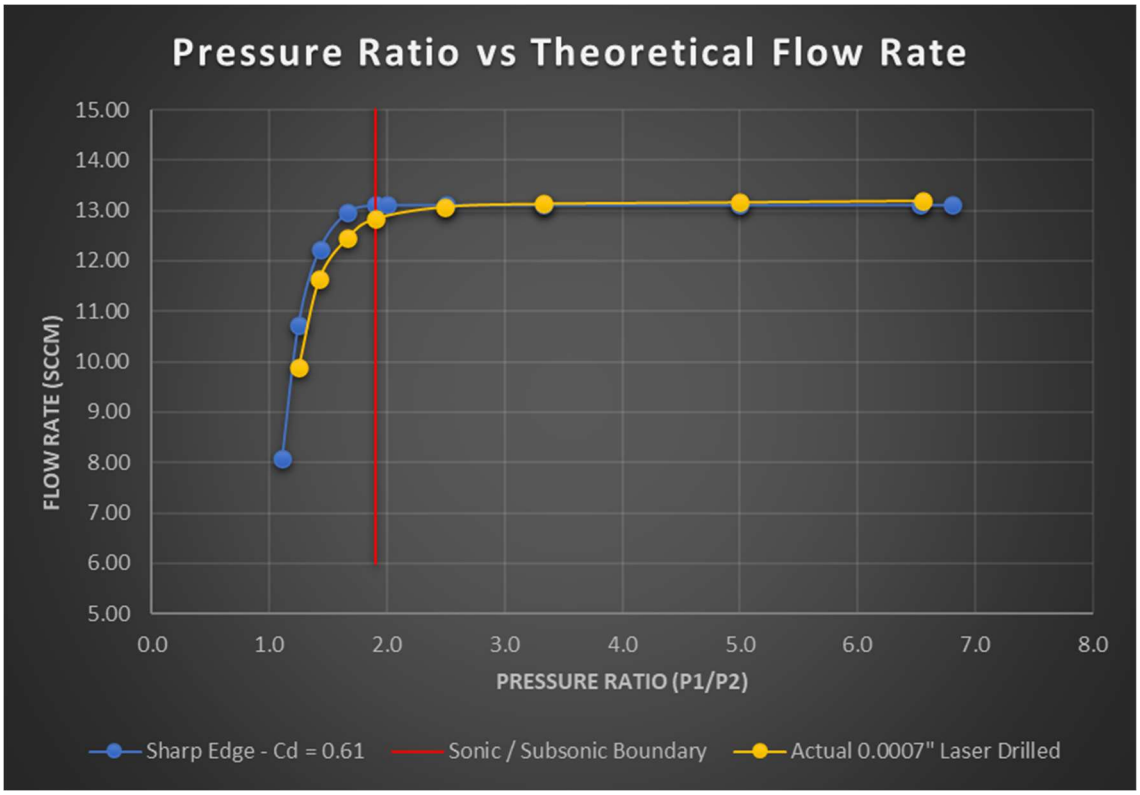

Figure 18: Plot of Experimental vs 0.65 Cd Theoretical

4. DISCUSSION

4.1 Discussion of Results and Analysis

The solutions within the theoretical portions of this report should be considered only an approximation to the solution since many assumptions were made that neglect real world compressible flow. For a more exact solution, the experimental data shall be consulted. With the aid of Gas Dynamics by Zucrow [1] and Mark's Handbook for Mechanical Engineers [2], we were able to derive and compare the mass flow a compressible fluid that is steady, reversible, isentropic, and one-dimensional which agreed as expected. The derivations, as with all governing equations, started out very complex, but with the methodical addition of our assumptions, the equations became manageable. Further derivations of the critical conditions or the sonic flow condition simplified the equations more when needed for those calculations.

We also must discuss the role of error prior to discussing the numerical results of the theory and experimental tests as this will show how well out results agree. Error associated with the derived equations compared to real world values include the fact that we considered an adiabatic perfect gas, an isentropic process, the flow was steady, one-dimensional, and reversible, and all body forces were neglected. These assumptions allow for the simplified use of the equations that allowed for the calculation of the flow at different pressure ratios through the orifice. We also considered an internal flow where the area change between the orifice and the internal flow area was neglected since the internal flow passage was much greater. The orifice was assumed to be either a sharp edge or a rounded edge since the edge condition of the experimental would be unknown until after

the flow testing. Errors associated with the flow test include all the measurement system accuracy (MSA) of the gauging used and the impurities in the Nitrogen gas used since it was not 100% pure.

It can be seen from Table 2 that for the sonic region of an orifice of 0.0007" with the inlet pressure of 100 psia, the flow rate is 12.30 SCCM for the assumption of a sharp edge orifice and 19.76 SCCM for a rounded edge orifice when in the sonic region (pressure ratio greater than or equal to 1.9). The subsonic region is further described in Table 3, which is not considered to be choked so the flow acts in a manner of an incompressible fluid where the flow rate decreases as the pressure ratio approaches unity. These curves agree with the theory established in Zucrow [1].

The manufacturing method used to produce the orifice was a laser. It was of interest to discover the smallest orifice that the laser system could produce as this is the most efficient method in obtaining a high restriction required for the propellant management systems. Other methods use multiple orifices in series, which take more time to build. The edge condition was unknown for such a small orifice with the ablation method of the laser. The vision system used gives a high accuracy of measurement, but also the visual geometry of the edge. It is shown to be sharp when considering the diameter of the orifice, but the edge was rounded slightly and included a deflection on one edge due to the melting of the material. The orifice is seen to be a tapered as shown in Figure 12 and the profile measured in Figure 13 which also includes a visual of the deflection on the left side of the hole. The heat marks on the face of the plate show potential location of high heat that has deformed the plate. The direction was marked prior to flow testing to ensure the sharpest edge possible, and the most drastic area change from the internal flow passage to the orifice.

The flow curve is shown comparatively to the sharp edge orifice in Figure 16 and 17. Figure 16 clearly shows that the orifice is closer to a sharp edge orifice with a coefficient of discharge of 0.61 rather than the rounded edge of 0.98. This tells us that the edge, though appearing round, is sharper. The magnification used can exaggerate the edge condition and any further visualizations should use this fact when evaluating. The agreement of the coefficient of discharge is present in the subsonic region by an average percent difference of 1.9%, which considering all of the assumptions and potential errors discussed is very accurate. It can be seen in Figure 17 that the deviation from the theoretical sharp edge curve increases as the flow approaches the theoretical sonic pressure ratio of 1.9. The average percent difference seen in the sonic region is 6.12% but is seen to continually increase instead of becoming a constant percent difference. At the pressure ratio of 1.9, the percent difference is 4.25% and ends at 6.99%. This means that the mass flow is not completely choked after the pressure ratio of 1.9 as the theory suggests. Extrapolation of the curve looks to show that this will continue as the pressure ratio increases.

When shifting the coefficient of discharge by 0.04 to a value of 0.65, the plot shifts and agrees more with the experimental values in the sonic region, but at the expense of agreement in the subsonic region. The average percent difference seen in the sonic region moves to 0.72% and the subsonic region is 5.75%. The largest percent difference being 8.32% at the pressure ratio of 1.25. With the behavior of the compressible fluid acting more like an incompressible fluid in the subsonic region, the edge condition looks to have an impact, which is why the agreement in both regions is not consistent with the theorized curve.

For real world values, it may be advantageous to define a minimum or maximum percent difference value that describes a choked condition since it will not be exact. Interestingly, it is also seen that the “knee” that theory shows the curve taking at the sonic boundary is not a hard bend at all, rather a gradual bend. With the importance of efficiency in the propellant management systems, it would be ideal to understand this “transition” region between the sonic and subsonic region to a higher degree.

When designing a miniature orifice for a propellant management system, the accuracy will need to be defined by the customer to determine if confirmation flow testing or prototyping is necessary or if the theorized calculations can be used. It has been shown that the most interest is the performance in the subsonic region as this will be the least efficient region, but the transition region should be considered as well when designing. When exact flow data is not necessary, the theoretical calculations can be used as it has been shown to have a close agreement to the experimental data. Since the agreement is so close, we can be confident that the calculations and derivations of the governing equations and the later simplified equations was completed correctly.

4.2 Future Work

Due to time constraints, the number of upstream pressures and orifice sizes were reduced to just one. Future work may include more upstream pressures to allow for high pressure ratios in the sonic region and more variation in the steps in the subsonic region. This will give a broader understanding of the impact of pressure. The orifice size, due to manufacturing backlogs, was kept at just 0.0007”, but larger orifices are of interest such as 0.0015” – 0.0065”.

For correlation purposes, other gases can be explored on the sharp edge orifice. This will allow an understanding of the performance of the gases of differing densities and purities. Some gases such as Helium are in short supply, so it would be advantageous to obtain data. Helium is also used as a correlating gas to many of the inert gases used in the propulsion systems such as Krypton and Xenon.

Lastly, the sharp edge orifice was targeted, but of interest is the impact of the lead in and lead out to the orifice rather than a sharp edge. This could be a great study to do numerically with computational fluid dynamics methods and software. There is also potential to study the impact of orifice in series and parallel as many systems may use such a setup.

REFERENCES

1. Zucrow, Maurice Joseph, and Joe D. Hoffman. Gas Dynamics. Wiley, 1976.
2. Sadegh, Ali M., and William M. Worek. Marks' Standard Handbook for Mechanical Engineers. McGraw-Hill Education, 2018.
3. https://www.theleeco.com/insights/selecting-accurate-flow-control-restrictors-for-electric-propulsion/
4. http://67.199.46.28/engineering/gases/gas-flow-characteristics.cfm
5. https://www.ddp.nl/wp-content/uploads/2020/07/Precision-Hydraulics-12th-Edition-2019.pdf
6. https://www.okeefecontrols.com/wp-content/uploads/Choked-Flow-of-Gases-pg-48.pdf
7. https://www.aft.com/documents/AFT-Modeling-Choked-Flow-Through-Orifice.pdf
8. https://www.nrc.gov/docs/ML1214/ML12142A162.pdf
9. http://willson.cm.utexas.edu/Teaching/Che253M/Files/EXP%202%20Compressible%20Gas%20Flow%2008-15.pdf
10. Goebel, Dan M, and Ira Katz. Fundamentals of Electric Propulsion : Ion and Hall Thrusters. Wiley, 2008. INSERT-MISSING-DATABASE-NAME, INSERT-MISSING-URL. Accessed 23 May 2022.
11. https://ntrs.nasa.gov/api/citations/19850010711/downloads/19850010711.pdf
12. http://mae-nas.eng.usu.edu/MAE_6530_Web/New_Course/Section3/compressible_orifice.pdf
13. https://www.nasa.gov/centers/glenn/technology/Ion_Propulsion1.html
14. https://www.osti.gov/servlets/purl/1031179#:~:text=The%20discharge%20coefficient%20for%20a,rounded%20edge%20orifice%20is%200.98.